

Coupling of small- and large-scale filament eruptions

Jia-Yan Yang¹, Yun-Chun Jiang¹, Bo Yang^{1,2}, Jun-Chao Hong¹ and Zhe Xu^{1,2}

¹ Yunnan Observatories, Chinese Academy of Sciences, Kunming 650011, China; yjy@ynao.ac.cn

² University of Chinese Academy of Sciences, Beijing 100049, China

Received 2014 October 27; accepted 2015 May 26

Abstract We present observations of the eruption of a large-scale quiescent filament (LF) that is associated with the formation and eruption of a miniature filament (MF). As a result of convergence and subsequent cancelation of opposite-polarity magnetic flux, MF was formed just below the spine of the LF's right segment. Probably triggered by a nearby newly emerging flux, MF underwent a failed eruption immediately after its full development, which first ejected away from the spine of LF and then drained back to the Sun. This eruption no sooner started than the overlying LF's right segment began to rise slowly and the LF's other parts were also disturbed, and eventually the whole LF erupted bodily and quickly. These observations suggest that the MF can serve as an intermediary that links the photospheric small-scale magnetic-field activities to the eruption of the overlying large filament. It appears that, rather than directly interacting with the supporting magnetic field of LF, small-scale flux cancelation and emergence in the LF's channel can manifest themselves as the formation and eruption of MF and so indirectly affect the stability of LF.

Key words: Sun: activity — Sun: filaments — Sun: magnetic fields

1 INTRODUCTION

The cause of filament instability is an important but still unresolved question. The stability of a filament is definitely determined by the corresponding magnetic environment, and thus the loss of stability may be greatly contributed by nearby photospheric magnetic-field displacements and changes (Schmieder 1990; Mackay et al. 2010). As for large-scale filaments in both quiet and active regions, previous studies have shown that their disturbances are closely related to pore birth and movement, as well as flux emergence and cancelation (Simon et al. 1986; Martin & Livi 1992; Wang et al. 1996; Jiang & Wang 2000, 2001; Kim et al. 2001; Zhang et al. 2001; Deng et al. 2002; Contarino et al. 2003; Sterling et al. 2007a,b; Sterling et al. 2011; Vemareddy et al. 2012; Wang & Muglach 2013). As a signature of steady magnetic reconnection in the low solar atmosphere (Wang & Shi 1993; Jiang et al. 2007), it is proposed that flux convergence and cancelation adjacent to filaments can not only lead to twist buildup in them (van Ballegooijen & Martens 1989) but also tether-cutting reconnection below them (Moore & Roumeliotis 1992), and thus play a role in their eruptions by introducing magnetohydrodynamic instability or by weakening their photospheric anchorages (Moore & Sterling 2006; Amari et al. 2010). As a strong catalyst for filament destabilization (Wang & Sheeley 1999), it is suggested that emerging flux can destabilize filaments by direct interaction with filament fields (Feynman & Martin 1995; Chen & Shibata 2000; Archontis & Hood 2008) or by indirect magnetic

coupling with the filament-carrying magnetic-field system (Balasubramaniam et al. 2011).

On the other hand, filaments show many similarities and common properties in a broad spectrum of sizes. Miniature filaments on the quiet Sun, the small-scale analog to large-scale ones, also lie above the magnetic polarity reversal boundaries between adjacent opposite-polarity fields, and their formation, maintenance, and eruption are also spatially associated with flux emergence and cancelation at these boundaries (Hermans & Martin 1986; Sakajiri et al. 2004; Zuccarello et al. 2007; Ren et al. 2008; Hong et al. 2011; Yang et al. 2012a; Yang et al. 2012b). Therefore, it appears that all scales of filament eruptions possibly have the same exterior agents and similar driving mechanisms. In a statistical study of 88 erupting $H\alpha$ miniature filaments, Wang et al. (2000) found that they had an average projected length of 1.9×10^4 km, a mean lifetime of 50 minutes from their first appearance to eruption, and perhaps most of the mass in the miniature filaments was transported to other magnetic structures rather than being ejected into the corona. More recently, Zhang et al. (2014) gave an example to show that chromospheric fibrils or miniature filaments can rise upward, merge into, and thus perturb an overlying prominence. Because of the huge difference in the lifetimes and spatial sizes of miniature and large-scale filaments, it seems that a miniature filament might erupt inside the channel of a large-scale filament with the involvement of flux cancelation and emergence in the photosphere. A rare event occurring on 2012 June

17 was just the case, in which the eruption of a large quiescent filament was preceded by the formation and eruption of a small filament below its spine. In this paper, we present the observational evidence to show that both the small- and large-scale filament eruptions might couple with each other via small-scale photospheric flux cancelation and emergence in the channel of the large-scale filament.

The paper is organized as follows: Section 2 describes the instrument and data we used, Section 3 gives the main results we obtained from the observations, while our conclusions and a brief discussion are given in Section 4.

2 OBSERVATIONS

The event was covered by observations from the Atmospheric Imaging Assembly (AIA; Lemen et al. 2012) and the Helioseismic and Magnetic Imager (HMI; Schou et al. 2012) on board the *Solar Dynamics Observatory* (SDO, Pesnell et al. 2012), the Solar Magnetic Activity Research Telescope (SMART) at Hida Observatory of Kyoto University in Japan (Ueno et al. 2004), and the Global Oscillation Network Group (GONG) at the National Solar Observatory (NSO). AIA takes full-disk images in 10 ultraviolet and extreme ultraviolet (EUV) wavelengths with a pixel size of $0.6''$ and a cadence of 12 s and we use the Level 1.5 304, 171 and 211 Å images to study the event. 304 Å (He II; $\log T = 4.7$) and 171 Å (Fe IX; $\log T = 5.8$) are mainly formed in the chromosphere and transition region, respectively, while 211 Å (Fe XIV; $\log T = 6.3$) is sensitive to responses in the flaring corona. HMI makes measurements of full-disk line-of-sight magnetic fields in the Fe I absorption line at 6173 Å with a spatial sampling of $0.5'' \text{ pixel}^{-1}$, a cadence of 45 s, and a precision of 10 G. SMART provides full-disk $H\alpha$ line-center and off-band ($\pm 0.5 \text{ \AA}$ and $\pm 0.8 \text{ \AA}$) images with a 1-minute cadence and a sampling of about $0.6'' \text{ pixel}^{-1}$, which are acquired using a Lyot filter with a bandpass of 0.25 \AA and recorded by a $4k \times 4k$ CCD. Because there are some gaps in the SMART data due to cloudy weather on June 17, we also examine full-disk $H\alpha$ line-center images provided by GONG, with a pixel size of $1''$ and a cadence of 1 minute. All of the images are differentially rotated to a reference time close to the event.

3 RESULTS

The large-scale quiescent filament “LF” was centered at about $S27^\circ W05^\circ$, with a longitudinal extension of about 30° from $E15^\circ$ to $W15^\circ$ and a latitudinal width of roughly 28° from $S12^\circ$ to 40° .

Figure 1 shows its general appearance and eruption process (also see the AIA 304 Å movie, named ‘2012.0617.AIA304.LF.mpeg,’ available in the online version of the journal). We see that LF was clearly visible in the first $H\alpha$ image (panel b1) but nearly disappeared in the second one (panel b2). When its pre-eruptive outlines determined from the 05:00 UT $H\alpha$ image were superimposed

on the corresponding HMI magnetogram (panel a), it became clear that LF was located along a polarity inversion line (PIL) of the photospheric magnetic field. It is noted that the photospheric magnetic-field evolution and activity in the region around LF were kept in a slow and weak level during the event. When we examined HMI observations, neither obvious large-scale flux cancelation nor obvious emergence was found. While LF disappeared gradually in $H\alpha$ images without any obvious eruption process, AIA 304 Å observations clearly reveal that it erupted bodily toward the northeastern direction after about 07:16 UT (indicated by the white thick arrows). As a normal feature of filament eruptions, this eruption was followed by EUV flare-like ribbons forming on the opposite sides of LF (indicated by the black thin arrows) and EUV post-eruptive loops gradually appeared to connect the ribbons (indicated by the black thick arrow). However, the most distinct characteristic of the event is that the LF eruption was preceded by the formation and eruption of a nearby miniature filament “MF” which will be discussed later. As enclosed by the blue box in panel c2, the MF eruption originated from a site centered at about $S23^\circ W08^\circ$ below the spine of LF’s right segment. Different from elongated brightenings or two-sided ejections associated with flux cancelation along the direction of filament channels shown by Wang & Muglach (2013) and the merging of rising miniature filaments into a larger prominence shown by Zhang et al. (2014), this eruption was also pointed toward nearly the same direction as LF’s eruption, and so did not directly collide or merge with the LF. Obviously, it had a very small scale relative to that of the LF. By using the potential-field source-surface (PFSS) software package available in SolarSoftWare (Schrijver & De Rosa 2003), the associated large-scale magnetic topology is obtained and the result is shown in Figure 2, along with superposed pre-eruptive $H\alpha$ outlines of LF and the maximum extent of the MF eruption obtained from the 06:00 UT AIA 304 Å image. It is found that, as expected, both LF and MF are held by an overarching magnetic arcade. Although the maximum extent of the MF eruption slightly exceeded the arcade, it began to drop after this (see the next two paragraphs for a detailed description of the MF eruption), indicating that most of the mass of MF is still confined to the interior of the arcade.

The tight temporal and spatial relationships between the MF and LF eruptions suggest that they might not be independent of each other but have a certain causal linkage. To verify such a possibility, time slices along the white thin arrows in Figure 1, “SR,” “SC,” “SLa,” “SLb,” and “SF,” are constructed over time from AIA 304 and 211 Å images. SF passes through the flare-like ribbons and the post-eruptive loops. SR/SC cross the centroid of MF/LF, SLa and SLb pass through LF’s left segment far away from MF, and they all point to LF’s eruption direction. Therefore, the SR slice reflects not only the eruption of MF but also that of LF’s right segment, while the SC, SLa and SLb slices reflect the eruption of LF’s central and left segments that deviated from MF by degrees.

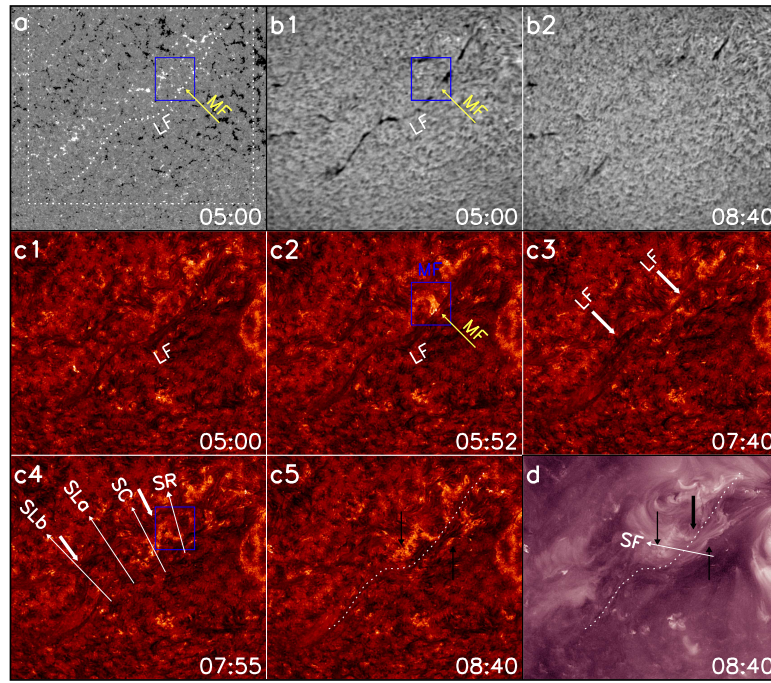


Fig. 1 HMI magnetogram (a), GONG $H\alpha$ (b1–b2), AIA 304 (c1–c5) and 211 Å (d) images, with a field of view (FOV) of $684'' \times 600''$. The eruption of a large quiescent filament “LF” was preceded by the eruption of a miniature filament “MF” located just under the spine of LF’s right segment. The 05:00 UT $H\alpha$ outlines of LF’s axis are plotted as white dashed curves. The thick white arrows indicate the erupting LF, and the thin and thick black arrows indicate the flare-like ribbons and post-eruptive loops, respectively. The white dashed box indicates the FOV of Fig. 2, and the blue boxes indicate the FOV of Fig. 4 where the MF eruption took place. The thin white arrows, “SR,” “SC,” “SLa,” “SLb,” and “SF,” indicate slit positions of the time slices shown in Fig. 3. (A 304 Å animation is available on <http://www.raa-journal.org/docs/Supp/2012.0617.AIA304.LF.mpeg>.)

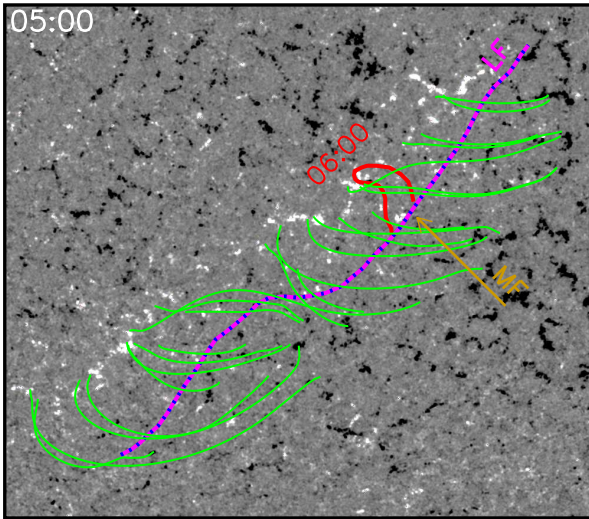


Fig. 2 Overlay of HMI magnetogram with the extrapolated PFSS field lines, along with superposed outlines of the initial LF (pink and blue) and the maximum extent of the erupted MF at 06:00 UT (red). LF is held by an arcade consisting of the green field lines, and the initial MF located inside the arcade is indicated by the brown arrow. The FOV, indicated by the white dashed box in Fig. 1, is $600'' \times 522''$. (Color version is online).

Figure 3 presents the results, in which the rising and erupting LF shows up as dark streaks. Clearly, the MF

eruption started at about 05:32 UT, reached the maximum projected height by 06:00 UT and then began to drop, and eventually ended at about 06:24 UT (panel a). MF thus underwent a failed eruption (Ji et al. 2003; Jiang et al. 2013) that was most likely blocked by the overlying arcade of LF and so mass of MF was still preserved inside it. The SR slice also shows that, prior to a quick eruption, the right segment of LF underwent a slow rise that started in the course of the MF eruption (panel a), clearly suggesting that the two filament eruptions might be closely related to each other. As compared with the SC, SLa, and SLb slices (panels b, c, and d respectively), however, it is surprisingly found that different segments of LF had different eruptive behaviors. Similar to the case of the right segment, the central and left segments of LF also showed two distinct stages of motion: a slow rise phase and a sudden eruption phase. The linear fittings to the rising/erupting dark streaks for each slice give the average rising/erupting velocity, V_1/V_2 , and their intersection defines the start time for each segment’s eruption, T_0 . As the distance from MF increased, V_1 decreased from 2.1 to 0.2 km s^{-1} while V_2 increased from 18.1 to 37.4 km s^{-1} , and the eruptive start time had a lag of 18 min from 07:16 to 07:34 UT. We thus believe that the MF eruption indeed exerted an effect on LF’s right segment, which first resulted in its slow rise and eruption, then disturbed the other parts of LF, and finally the entire LF progressively erupted. It is also clear that both the flare-like

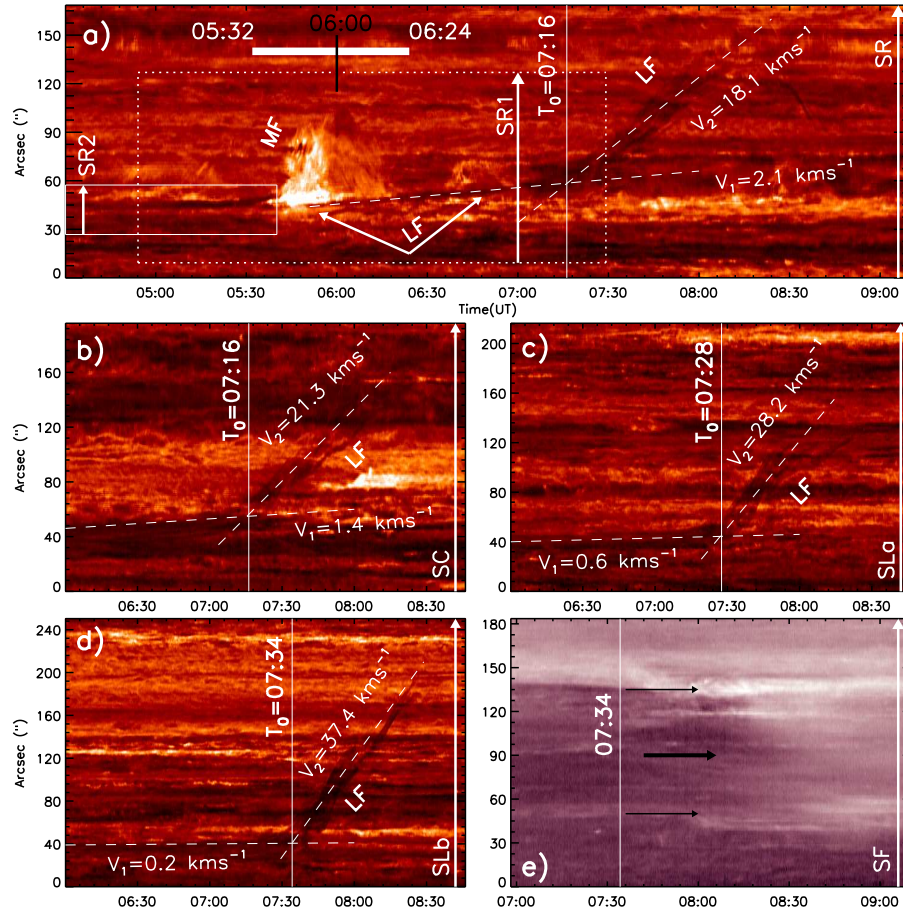


Fig. 3 Time slices from AIA 304 Å images for the SR (a), SC (b), SLa (c), and SLb (d) slits, and from AIA 211 Å images for the SF slit (e) shown in Fig. 1, in which the spatial slices are laid adjacent from left to right and the distances are measured along the slit directions indicated by the arrows. The dashed lines mark the linear fittings to the rising/erupting LF’s segment, and V_1 , V_2 and T_0 are defined in the text. In (a), the horizontal bar indicates the duration of the MF eruption, and some critical moments are marked by the vertical bars and described in the text. The dotted/solid boxes indicate two smaller regions given in Fig. 6, which present the time slices that are cut along two segments of SR in the FOVs of Figs. 4 and 5, “SR1” and “SR2,” respectively. The two white arrows indicate the slow rise of LF’s right segment. In (e), the thin and thick black arrows indicate the flare-like ribbons and post-eruptive loops, respectively.

ribbons and post-eruptive loops appeared after the bodily rapid eruption of LF (panel e).

By carefully examining $H\alpha$ and EUV observations, we can investigate further details about the MF eruption. This is illustrated by the close-up view of AIA 304 Å and SMART $H\alpha$ images in Figure 4 (also see the AIA 304 Å movie, named ‘2012.0617.AIA304.MF.mpeg’, available in the online version of the journal). From the movie, we can see that the MF eruption appears to be a jet-like one, and counterclockwise untwisting motion is also observed. To clearly display the dynamic characteristics of the eruption and its action on LF’s right segment, $H\alpha$ line-of-sight velocity maps were made by means of a subtraction technique in nearly simultaneous SMART off-band $H\alpha$ image pairs (Leighton et al. 1962), and the velocity pictures constructed by subtracting red-wing from blue-wing images at $H\alpha \pm 0.5 \text{ \AA}$ are presented (panels c1–c7), in which white/black areas show falling/rising materials and grey areas indicate no line-of-sight motion in the filaments. As

mentioned above, we can regard 05:32/06:00/06:24 UT as the start/drop/end times of the MF eruption. Before its eruption, MF intersected with LF at an appropriate angle conducive to distinguishing it from LF in the 304 Å image (indicated by the arrow in panel a1), while in the simultaneous $H\alpha$ image it was ambiguous, maybe due to its tiny size (panel b1). However, MF was also discernible in several $H\alpha$ line-center images at its early eruptive phase. At 05:35 UT when MF began to violently erupt as revealed by the appearance of an elongated blueshift signature (panel c2), it appeared at the $H\alpha$ line-center and had a similar shape to that at 304 Å (indicated by the arrows in panels a2 and b2). Afterwards, when the erupting MF still displayed blueshifts (panels c3–c4) and could be distinguished at the $H\alpha$ line-center (panels b3–b4), it showed up as a bright feature at 304 Å (panels a3–a4), probably indicating that the eruption involved the ionizing and heating of the filament plasma. Finally, the eruption gradually faded away (panels a5, b5, and c5) but LF’s right segment

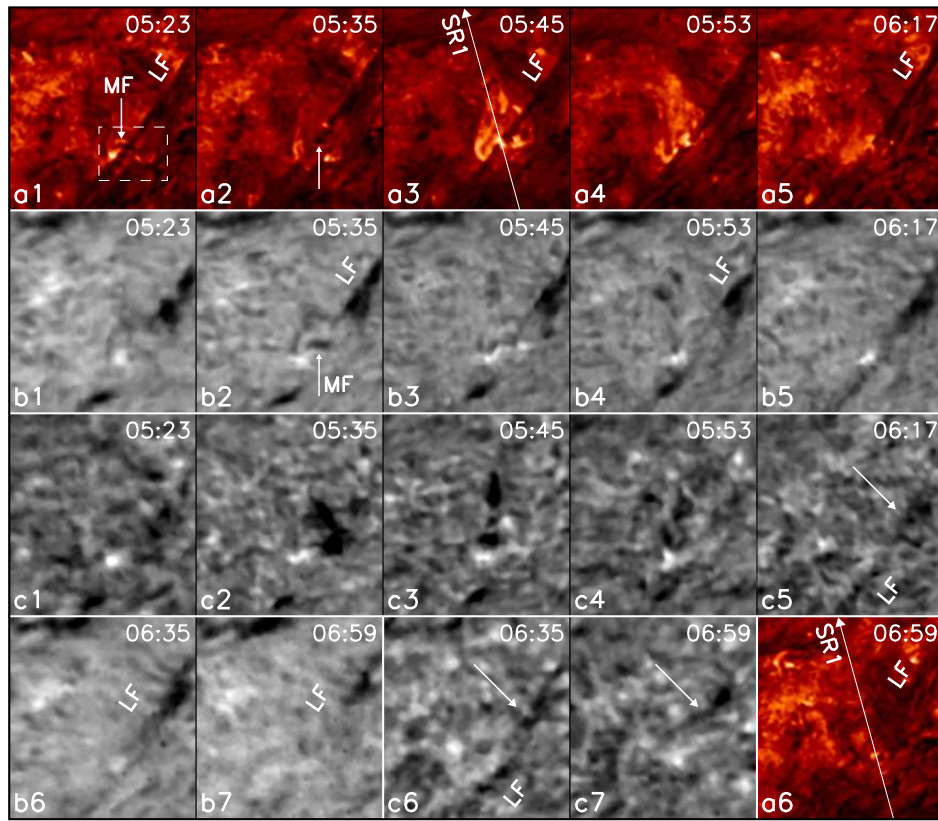


Fig. 4 AIA 304 Å (a1–a6) and SMART H α line-center (b1–b7) images, as well as Doppler subtractions of SMART H α \pm 0.5 Å images with white/black showing redshifts/blueshifts (c1–c7). MF underwent a clear eruption before the overall eruption of LF. The FOV, indicated by the blue boxes in Figure 1, is $105'' \times 114''$. “SR1,” a segment of the SR slit that is cut (see Fig. 1) in this FOV, indicates the slit position of a time slice shown in Fig. 6. The white dashed box indicates the FOV of Fig. 5. (A 304 Å animation is available on <http://www.raa-journal.org/docs/Supp/2012.0617.AIA304.MF.mpeg>.)

showed a faint blueshift signature (indicated by the arrow in panel c5). Consistent with the slow rise of LF’s right segment shown in Figure 3, such a blueshift persisted after the MF eruption ended (indicated by the arrows in panels c6–c7), and the nearby LF had significant morphologic changes as compared with the pre-eruptive one (see panels a6 and b6–b7). These observations again suggest that the MF eruption indeed affected the stability of LF’s right segment and thus might be a key driving agent for the whole LF eruption.

Owing to the short mean lifetime of miniature filaments, it is also easy to trace the complete formation process of MF and thus to further study the relationship with the corresponding photospheric small-scale magnetic-field activities. This is shown by the close-up view of representative AIA 171 and 304 Å images and HMI magnetograms in Figure 5 (also see the HMI magnetogram movie, named ‘2012.0617.HMI.mag.mpeg’, available in the online version of the journal). Although it is difficult to determine the exact start time of the MF formation due to its very small size and changes in brightness, we can estimate it first appearing at about 05:00 UT as a small dark feature from the 171 and 304 Å movies (panels a1 and b1). Then it grew toward both the east and west with a curved path in

less than 30 min, and reached its maximum extent by about 05:23 UT with a length of about 2.1×10^4 km in the 171 Å image (panel a3). This is comparable with the average projected length of 1.9×10^4 km for miniature filaments (Wang et al. 2000). Consistent with the preferential pattern of a sinistral filament in the southern hemisphere, it is noted that MF exhibited an S shape at this time. Therefore, MF had a lifetime of about 32 min from its first appearance (05:00 UT) to when its eruption started (15:32 UT), also comparable with the 50-min mean lifetime of miniature filaments given by Wang et al. (2000). HMI magnetic-field observations show that the MF formation was associated with convergence and then cancellation of three opposite-polarity magnetic flux patches, “p1,” “p2,” and “n,” and its eruption might be triggered by a newly emerging flux. As indicated by the diagonal-dashed lines, the negative flux patch n moved eastward while the large/small positive flux patch p1/p2 moved northwestward/southward, thus they got closer to and met each other just before MF started to form (panel c1–c3). Then the areas of n and p2 continuously decreased, and finally disappeared completely (panels c5 and c6). When the 05:23 UT 171 Å outlines of MF’s axis were superimposed on the simultaneous HMI magnetogram (panel c4), we see that MF roughly

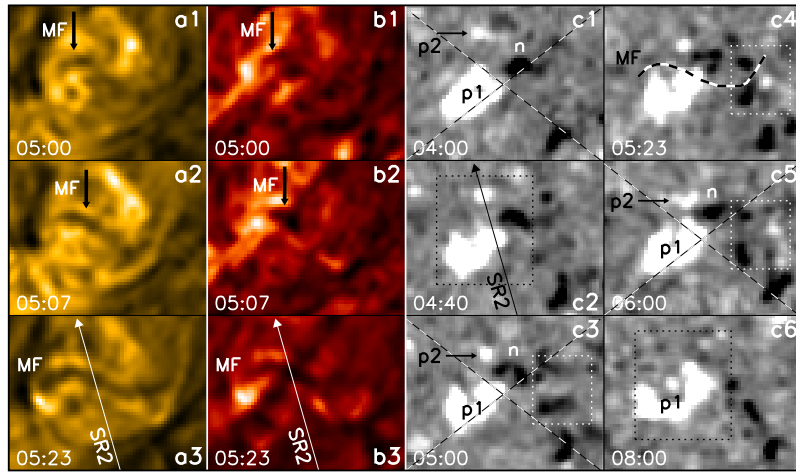


Fig. 5 AIA 171 (a1–a3) and 304 Å (b1–b3) images showing the MF formation, and HMI magnetogram (c1–c6) showing the corresponding evolution of nearby photospheric small-scale magnetic field. The FOV, indicated by the white dashed box in Figure 4, is $38'' \times 30''$. “SR2,” a segment of the SR slit that is cut (see Fig. 1) in this FOV, indicates a slit position of time slices shown in Fig. 6. The diagonal-dashed lines in panels c1, c3 and c5 help to show the convergence and cancellation of three opposite-polarity magnetic flux patches, “p1,” “p2,” and “n.” The white-dotted boxes in panels c3–c5 enclose the area of the newly emerging flux. (An HMI magnetogram animation is available on <http://www.raa-journal.org/docs/Supp/2012.0617.HMI.mag.mpeg>.)

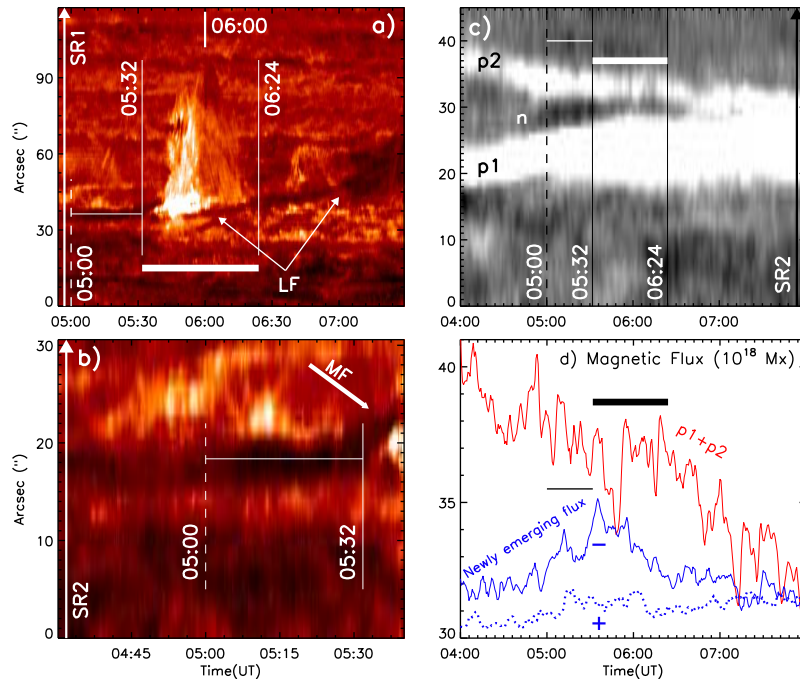


Fig. 6 Time slices from AIA 304 Å images for the SR1 (a) and SR2 (b) slits (see Figs. 4 and 5), time slice from HMI magnetograms for the SR2 (c) slit (see Fig. 5), along with changes of magnetic flux within the black/white-dotted boxes in Fig. 5 (d). The thin/thick horizontal bars indicate the durations of the MF formation/eruption, and some critical moments are marked by the vertical bars and described in the text. The thick arrow in *b* indicates the erupting MF, and the two thin arrows in *a* indicate the slow rise of LF’s right segment. To improve clarity, the total values for the positive fluxes are plotted in *d*, and the positive/negative flux values for the newly emerging flux are shifted 30/28 on the vertical scale.

resided above the PIL between these opposite-polarity flux patches. These observations thus support the idea that convergence and cancellation of opposite-polarity flux are not only necessary conditions for filament formation (Martin 1998) but can also disturb miniature filaments (Hermans

& Martin 1986, and the references therein). In the course of the MF formation and eruption, a newly emerging flux also appeared around the western end of the MF. This is indicated by the white-dotted boxes in panels c3–c5. Compared with observations before the MF formation (c1–

c2), the flux emergence can obviously be seen, and as is common in emerging flux, it consisted of opposite-polarity patches that separated from each other. As suggested by previous observations (Moore & Roumeliotis 1992; Jiang et al. 2007), such an emergence may play a role in triggering the MF eruption by modifying its line-tying condition.

The above cancelation process can be displayed more clearly by a time slice made from HMI magnetograms along a segment of the SR slit that is cut (see Fig. 1). “SR2” in Figure 5 passes through not only the initial formation site of MF but also *p1*, *p2*, *n* and their meeting site. Figure 6 presents the result, along with changes of magnetic flux within the black/white-dotted boxes covering the canceling/emerging flux regions. Because there was negative flux moving into the black-dotted box, changes of negative flux in it are not presented. To compare with the details of the MF formation and eruption, two smaller regions in the SR time slice (enclosed by the dashed/solid boxes in Fig. 3a) are also shown. They represent the time slices along two segments of the SR slit that are cut, i.e., SR2 in Figure 5 and SR1 along the eruption direction of MF in Figure 4, respectively. In agreement with the description above, MF was formed from 05:00 to 05:32 UT (panel b) and then erupted between 05:32 and 06:24 UT (panel a), while LF rose slowly (indicated by the arrows in panel a) in the process of the MF eruption. In the HMI slice (panel c), *n* first bumped into SR2 just before the MF began to form, and then the cancelation of *n* with the converging *p1* and *p2*, as well as the resulting disappearance of *n*, were clearly discernible in the course of the MF eruption). When the positive flux in the canceling region showed a tendency of continuous decrease, both the positive and negative flux in the emerging region first increased and then decreased simultaneously (panel d), suggesting that the MF formation and eruption were closely associated with the nearby flux cancelation and emergence.

4 CONCLUSIONS AND DISCUSSION

By using high-cadence and high-resolution observations, we present a detailed study on the relationship between the small MF and large LF eruptions, as well as the photospheric magnetic-field evolution around MF. The main results are as follows. (1) The LF eruption was preceded by the formation and eruption of MF that was located just below the spine of LF’s right segment. MF had a very small spatial scale and a short lifetime relative to those of LF, and, obviously different from the full LF eruption, its eruption was a failed case. (2) Followed by the bodily quick eruption of LF, its right segment showed a slow rise and the other parts were also disturbed in the course of the MF eruption. (3) The MF formation and eruption were closely associated with the convergence and cancelation of opposite-polarity magnetic flux, as well as a newly emerging flux. Because of the high temporal and spatial closeness of the two eruptions, we pay special attention to their causal connection, and reasonably speculate that the LF eruption was caused by indirect magnetic coupling of

its supporting magnetic field with that of the erupting MF. It seems that the two eruptions can be regarded as an integral process coordinated by changes in the small-scale photospheric magnetic field around MF, in which the MF eruption acted as a vehicle that reflects the effect of these small-scale photospheric activities on the stability of LF.

Because the disruption of the large-scale filament magnetic field can be driven by changes in the small-scale photospheric field (Raadu et al. 1988), it is unsurprising that in our case the flux convergence, cancelation, and emergence around the small MF might play important roles in disturbing the large LF. However, our observations indicate that the results of these small-scale photospheric activities were the MF formation and eruption rather than the direct magnetic interaction with the surrounding field of LF. As shown by previous observations (Hermans & Martin 1986, and the references therein), it is not uncommon that these photospheric activities can lead to the MF formation and eruption. Because the size/lifetime of LF were much larger/longer than those of MF, it is reasonable to imagine that LF was much more highly overlying these photospheric activities (Rompolt 1990). This configuration allowed the lower MF to form in a small spatial range below LF. As suggested by Sakajiri et al. (2004), the MF formation might represent the buildup and accumulation process of magnetic free energy and/or helicity introduced by the small-scale photospheric activities. It is very likely that, similar to the situation of filament eruptions initiated by newly emerging bipoles (Wang & Sheeley 1999), the consequent MF eruption could disturb the overlying arcade of LF, i.e., divert the flux overlying LF sideways or to greater heights, and it may be the main reason for LF’s eruption. On the other hand, the failed eruption of MF implies that the stored energy and helicity would be injected from small to large spatial scale (Raouafi et al. 2010; Xue et al. 2014) but still limited below the overlying arcade of LF, and thus might add more twist/shear or helicity to LF and could also affect its stability. In this sense, the above scenario is similar to so-called flux feeding from chromospheric fibrils or miniature filaments underneath that might be an important mechanism to trigger coronal eruptions (Zhang et al. 2014). In our case, however, the small-scale photospheric activities do not interact with LF’s field directly (Balasubramaniam et al. 2011) but manifest themselves as the MF formation and eruption, during which magnetic energy and complexity are first stored in the layers near the photosphere and then released and transported upward into the corona. So, neither twist buildup within LF’s magnetic system itself (van Ballegooijen & Martens 1989) nor tether-cutting reconnection below LF that can change, and weakening its photospheric linkage (Moore & Roumeliotis 1992) is needed. If so, all small-scale eruptions occurring inside the spatial range of arcades overlying large-scale filaments could be treated as mediums that connect photospheric activities to the filaments and would make larger or smaller contributions to their disturbance. Clearly, how

this mechanism functions in disturbing a large-scale filament needs to be detailed further.

Acknowledgements We thank the anonymous referee for providing suggestions and comments that improved the presentation of this paper. The authors thank the *SDO* team, the SMART team, and the GONG/NSO consortium for providing the excellent data. SMART is operated under an open data policy at Hida Observatory of Kyoto University, Japan. This work is supported by the National Natural Science Foundation of China (NSFC, Grant Nos. 11273056, 11473065 and 11333007).

References

- Amari, T., Aly, J.-J., Mikic, Z., & Linker, J. 2010, *ApJ*, 717, L26
- Archontis, V., & Hood, A. W. 2008, *ApJ*, 674, L113
- Balasubramaniam, K. S., Pevtsov, A. A., Cliver, E. W., Martin, S. F., & Panasenco, O. 2011, *ApJ*, 743, 202
- Chen, P. F., & Shibata, K. 2000, *ApJ*, 545, 524
- Contarino, L., Romano, P., Yurchyshyn, V. B., & Zuccarello, F. 2003, *Sol. Phys.*, 216, 173
- Deng, Y., Lin, Y., Schmieder, B., & Engvold, O. 2002, *Sol. Phys.*, 209, 153
- Feynman, J., & Martin, S. F. 1995, *J. Geophys. Res.*, 100, 3355
- Hermans, L. M., & Martin, S. F. 1986, in *NASA Conference Publication*, 2442, ed. A. I. Poland, 369
- Hong, J., Jiang, Y., Zheng, R., et al. 2011, *ApJ*, 738, L20
- Ji, H., Wang, H., Schmahl, E. J., Moon, Y.-J., & Jiang, Y. 2003, *ApJ*, 595, L135
- Jiang, Y., & Wang, J. 2000, *A&A*, 356, 1055
- Jiang, Y., & Wang, J. 2001, *A&A*, 367, 1022
- Jiang, Y.-C., Shen, Y.-D., & Wang, J.-X. 2007, *ChJAA (Chin. J. Astron. Astrophys.)*, 7, 129
- Jiang, Y., Hong, J., Yang, J., et al. 2013, *ApJ*, 764, 68
- Kim, J.-H., Yun, H. S., Lee, S., et al. 2001, *ApJ*, 547, L85
- Leighton, R. B., Noyes, R. W., & Simon, G. W. 1962, *ApJ*, 135, 474
- Lemen, J. R., Title, A. M., Akin, D. J., et al. 2012, *Sol. Phys.*, 275, 17
- Mackay, D. H., Karpen, J. T., Ballester, J. L., Schmieder, B., & Aulanier, G. 2010, *Space Sci. Rev.*, 151, 333
- Martin, S. F. 1998, *Sol. Phys.*, 182, 107
- Martin, S. F., & Livi, S. H. B. 1992, in *Lecture Notes in Physics*, Berlin Springer Verlag, 399, IAU Colloq. 133: Eruptive Solar Flares, eds. Z. Svestka, B. V. Jackson, & M. E. Machado, 33
- Moore, R. L., & Roumeliotis, G. 1992, in *Lecture Notes in Physics*, Berlin Springer Verlag, 399, IAU Colloq. 133: Eruptive Solar Flares, eds. Z. Svestka, B. V. Jackson, & M. E. Machado, 69
- Moore, R. L., & Sterling, A. C. 2006, *Washington DC American Geophysical Union Geophysical Monograph Series*, 165, 43
- Pesnell, W. D., Thompson, B. J., & Chamberlin, P. C. 2012, *Sol. Phys.*, 275, 3
- Raadu, M. A., Schmieder, B., Mein, N., & Gesztelyi, L. 1988, *A&A*, 197, 289
- Raouafi, N.-E., Georgoulis, M. K., Rust, D. M., & Bernasconi, P. N. 2010, *ApJ*, 718, 981
- Ren, D. B., Jiang, Y. C., Yang, J. Y., et al. 2008, *Ap&SS*, 318, 141
- Rompolt, B. 1990, *Hvar Observatory Bulletin*, 14, 37
- Sakajiri, T., Brooks, D. H., Yamamoto, T., et al. 2004, *ApJ*, 616, 578
- Schmieder, B. 1990, in *Lecture Notes in Physics*, Berlin Springer Verlag, 363, IAU Colloq. 117: Dynamics of Quiescent Prominences, eds. V. Ruzjak, & E. Tandberg-Hanssen, 85
- Schou, J., Scherrer, P. H., Bush, R. I., et al. 2012, *Sol. Phys.*, 275, 229
- Schrijver, C. J., & De Rosa, M. L. 2003, *Sol. Phys.*, 212, 165
- Simon, G., Gesztelyi, L., Schmieder, B., & Mein, N. 1986, in *NASA Conference Publication*, 2442, ed. A. I. Poland, 229
- Sterling, A. C., Harra, L. K., & Moore, R. L. 2007a, *ApJ*, 669, 1359
- Sterling, A. C., Moore, R. L., Berger, T. E., et al. 2007b, *PASJ*, 59, 823
- Sterling, A. C., Moore, R. L., & Freeland, S. L. 2011, *ApJ*, 731, L3
- Ueno, S., Nagata, S., Kitai, R., & Kurokawa, H. 2004, in *Astronomical Society of the Pacific Conference Series*, 325, *The Solar-B Mission and the Forefront of Solar Physics*, eds. T. Sakurai, & T. Sekii, 319
- van Ballegooijen, A. A., & Martens, P. C. H. 1989, *ApJ*, 343, 971
- Vemareddy, P., Maurya, R. A., & Ambastha, A. 2012, *Sol. Phys.*, 277, 337
- Wang, J., & Shi, Z. 1993, *Sol. Phys.*, 143, 119
- Wang, J., Shi, Z., & Martin, S. F. 1996, *A&A*, 316, 201
- Wang, J., Li, W., Denker, C., et al. 2000, *ApJ*, 530, 1071
- Wang, Y.-M., & Sheeley, Jr., N. R. 1999, *ApJ*, 510, L157
- Wang, Y.-M., & Muglach, K. 2013, *ApJ*, 763, 97
- Xue, Z. K., Yan, X. L., Qu, Z. Q., Xu, C. L., & Zhao, L. 2014, *Ap&SS*, 353, 357
- Yang, J., Jiang, Y., Yang, B., et al. 2012a, *New Astron.*, 17, 732
- Yang, J.-Y., Jiang, Y.-C., Yang, D., et al. 2012b, *RAA (Research in Astronomy and Astrophysics)*, 12, 300
- Zhang, J., Wang, J., & Nitta, N. 2001, *ChJAA (Chin. J. Astron. Astrophys.)*, 1, 85
- Zhang, Q., Liu, R., Wang, Y., et al. 2014, *ApJ*, 789, 133
- Zuccarello, F., Battiatto, V., Contarino, L., Romano, P., & Spadaro, D. 2007, *A&A*, 468, 299